Mechatronics 20 (2010) 656–665

Contents lists available at ScienceDirect

Mechatronics

journal homepage: www.elsevier.com/locate/mechatronics

Active damping of a piezoelectric tube scanner using self-sensing piezo actuation

S. Kuiper [a], G. Schitter [a,b,*]

[a] Delft Center for Systems and Control, Precision and Microsystems Engineering, Delft University of Technology, Mekelweg 2, 2628CD Delft, The Netherlands
[b] Automation and Control Institute, Vienna University of Technology, Gusshausstrasse 27-29, 1040 Vienna, Austria

ARTICLE INFO

Article history:
Received 31 December 2009
Accepted 11 July 2010

Keywords:
Atomic Force Microscopy
Piezoelectric actuators
Self-sensing actuation

ABSTRACT

In most Atomic Force Microscopes (AFM), a piezoelectric tube scanner is used to position the sample underneath the measurement probe. Oscillations stemming from the weakly damped resonances of the tube scanner are a major source of image distortion, putting a limitation on the achievable imaging speed. This paper demonstrates active damping of these oscillations in multiple scanning axes without the need for additional position sensors. By connecting the tube scanner in a capacitive bridge circuit the scanner oscillations can be measured in both scanning axes, using the same piezo material as an actuator and sensor simultaneously. In order to compensate for circuit imbalance caused by hysteresis in the piezo element, an adaptive balancing circuit is used. The obtained measurement signal is used for feedback control, reducing the resonance peaks in both scanning axes by 18 dB and the cross-coupling at those frequencies by 30 dB.

Experimental results demonstrate a significant reduction in scanner oscillations when applying the typical triangular scanning signals, as well as a strong reduction in coupling induced oscillations. Recorded AFM images show a considerable reduction in image distortion due to the proposed control method, enabling artifact free AFM-imaging at a speed of 122 lines per second with a standard piezoelectric tube scanner.

1. Introduction

Atomic Force Microscopy (AFM) [1] is an important tool in nanotechnology to provide images up to atomic resolution under several environmental conditions. In AFM, the sample topography is measured by a very sharp tip which is mounted on the free end of a small cantilever beam, as depicted in Fig. 1. By probing the surface topography with the tip while the sample is scanned in a raster scan pattern, a topographical image of the sample is recorded. To provide the positioning of the sample in all three spatial directions, most commercially available AFM setups use piezoelectric tube scanners [2], as shown in Fig. 1, because of their simple design, high resolution and low cost. These tube scanners consist of a tube of piezoelectric material with segmented electrodes on the side. In order to provide the lateral scanning motion, a voltage is applied over the electrodes which induces a bending motion of the tube. One major drawback of these piezoelectric tube scanners, however, are their weakly damped resonances. Excitation of these resonances induces scanner oscillations, which is a major cause of image distortion in AFM-imaging [3,4]. To prevent excitation of these oscillations the line scan rate is limited to about 1% of the scanners fundamental resonance frequency, making AFM-imaging a relatively time consuming process taking in the order of several minutes per image for conventional AFM setups [5,6].

In literature several methods can be found to compensate for the scanner oscillations, which can be subdivided in feedforward and feedback control methods [7,8]. With feedforward techniques the input signal is shaped such that the scanner resonances are not excited, which result in a significant enhancement of the achievable scan speed [3,4,9,10]. Feedforward methods, however, do not apply direct damping to the scanners resonant modes, such that these may still be excited by environmental noise. Furthermore, feedforward methods are relatively sensitive for changes of the system dynamics, occurring for instance when changing the sample mass resulting in a shift of the resonance frequency [4].

Feedback control methods [11–13] can account for system uncertainty and allow active damping of the resonant modes. However, as conventional feedback control methods require the use of position sensors, e.g. capacitive or optical, application of feedback control is cost-intensive. In [14,15] the use of external position sensors is omitted by using part of the available electrode surface of the piezoelectric tube for sensing, measuring the charge induced on these passive electrodes by the bending of the tube.

* Corresponding author at: Delft Center for Systems and Control, Precision and Microsystems Engineering, Delft University of Technology, Mekelweg 2, 2628CD Delft, The Netherlands. Tel.: +43 (0)1 588 01 37610.
E-mail addresses: stefan.kuiper@tudelft.nl (S. Kuiper), schitter@acin.tuwien.ac.at (G. Schitter).

0957-4158/$ - see front matter © 2010 Elsevier Ltd. All rights reserved.
doi:10.1016/j.mechatronics.2010.07.003

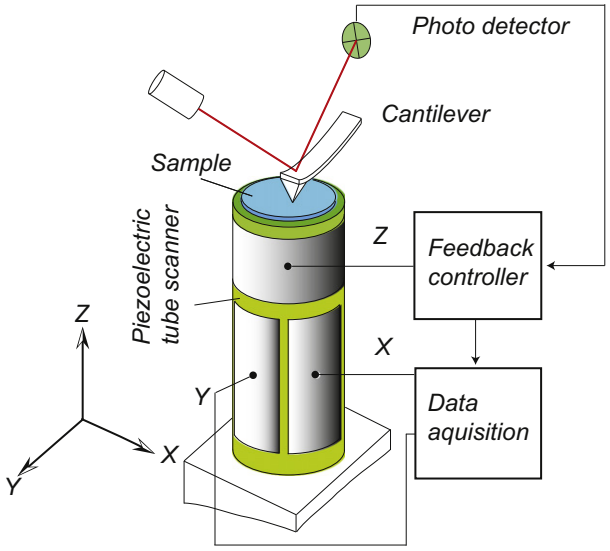

Fig. 1. Schematic of an Atomic Force Microscope with a piezoelectric tube scanner for the positioning of the sample.

Although this technique enables active damping of the fundamental resonances, the maximum scan range is compromised as not the whole available electrode surface is used for actuation. In [16,17], a reduction of scanner oscillations is achieved by connecting a shunt impedance in parallel with the scan-electrodes. Although most of the contributions mentioned above are mainly concerned with compensation of the oscillations in the fast scanning axis, mechanical cross-couplings in the piezoelectric tube can induce oscillations in the slow scanning axis as well. This becomes even more evident when image rotation in applied, as in that case the fast and slow scanning directions are not in line with the position axes of the piezoelectric tube scanner.

In this contribution, self-sensing actuation and damping of both scanning axes of a piezoelectric tube scanner is presented, reducing the resonance peaks in both scanning axes as well as the resonance induced cross-coupling without the need for additional position sensors. In Sections 2 and 3 self-sensing actuation and a method to compensate for circuit imbalance are described. The design of the feedback controller for active damping of the scanner resonances is discussed in Section 4, and the implementation of the proposed control system is presented in Section 5. The achieved damping and higher scan speed is demonstrated experimentally in Section 6, showing a significant reduction in scanner oscillations at fast scanning. AFM images recorded at 122 lines per second demonstrate the significant reduction of the scanner oscillations and improvement in image quality.

2. Self-sensing piezo actuation

Self-sensing piezo actuation allows to use a piezoelectric element for both actuation and sensing simultaneously [18].

2.1. Principle of self-sensing actuation

A piezoelectric element is a transducer, that transfers energy from the electrical domain to mechanical domain and vice versa by the following relations [19]:

$$\begin{bmatrix} x(t) \\ q(t) \end{bmatrix} = \begin{bmatrix} K^{-1} & d \\ d & C_p \end{bmatrix} \begin{bmatrix} f_p(t) \\ u_p(t) \end{bmatrix}, \tag{1}$$

with displacement $x(t)$, charge $q(t)$, external force $f_p(t)$ acting on the piezo element, voltage $u_p(t)$ over the piezo element, mechanical

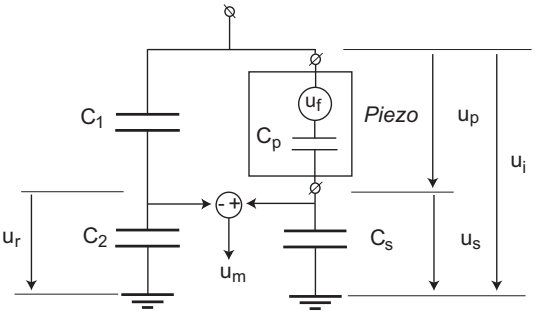

Fig. 2. Scheme of self-sensing piezo actuation. The capacitance ratios are chosen as $C_P/C_s = C_1/C_2$.

stiffness K, piezoelectric constant d, and capacitance C_p. Rewriting the second row of Eq. (1) shows that the voltage over the piezo is depending on the external forces acting on the piezo:

$$u_p(t) = \frac{1}{C_p} q(t) - \frac{d}{C_p} f_p(t). \tag{2}$$

Therefore, in the electrical domain the piezo element may be seen as a capacitor C_p in series with a voltage source, of which the voltage is induced by the external forces acting on the piezo element. This allows using a piezo element as a force sensor. By connecting the piezoelectric element in a capacitive bridge circuit, as first described in [18], the sensing capabilities can be combined with actuation. Fig. 2 shows this capacitive bridge circuit, where the piezo element is connected in series with a capacitor C_s. Using Eq. (2), the voltage over capacitor C_s can be calculated as:

$$u_s(t) = u_i(t) - u_p(t) = u_i(t) - \frac{1}{C_p} q(t) + \frac{d}{C_p} f_p(t), \tag{3}$$

where $u_i(t)$ is the driving voltage over the bridge circuit. As the capacitor C_s is in series with the piezo element, the charge $q(t)$ in both elements must be equal, therefore Eq. (3) can be rewritten as:

$$\begin{aligned} u_s(t) &= \frac{1}{C_s} q(t) = \frac{C_p}{C_p + C_s} \left(u_i(t) + \frac{d}{C_p} f_p(t) \right) \\ &= \frac{C_p}{C_p + C_s} \cdot u_i(t) + \frac{d}{C_p + C_s} \cdot f_p(t), \end{aligned} \tag{4}$$

i.e. the voltage measured over the capacitor C_s in series with the piezo consist of a part induced by the driving voltage $u_i(t)$ and a part induced by the external forces $f_p(t)$ acting on the piezo. In the capacitive bridge circuit as shown in Fig. 2, the measurement voltage $u_m(t)$ is obtained by measuring the voltage over the bridge circuit: $u_m(t) = u_s(t) - u_r(t)$. By choosing the capacitor ratios in both branches of the bridge circuit equal $\frac{C_p}{C_s} = \frac{C_1}{C_2}$ the signal components which are directly stemming from the driving voltage $u_i(t)$ are being canceled, i.e. measurement voltage $u_m(t)$ is directly proportional to the force $f_p(t)$ acting on the piezo element;

$$\begin{aligned} u_m(t) &= u_s(t) - u_r(t) \\ &= \left(\frac{C_p}{C_p + C_s} \cdot u_i(t) + \frac{d}{C_p + C_s} \cdot f_p(t) \right) - \frac{C_1}{C_1 + C_2} \cdot u_i(t) \\ &= \frac{d}{C_p + C_s} \cdot f_p(t). \end{aligned} \tag{5}$$

How force $f_p(t)$ now corresponds to the displacement of the actuator depends on the structure in which the piezo element is mounted. In a tube scanner used for AFM, the piezoelectric tube is directly actuating the mass of the sample, which is typically on the same order of magnitude as the mass of the piezo itself. Therefore, the force acting on the piezo element is directly proportional to the acceleration and damping forces of the moving masses; $f_p(t) = -M \frac{dx^2}{d^2t} - \beta \frac{dx}{dt}$, with

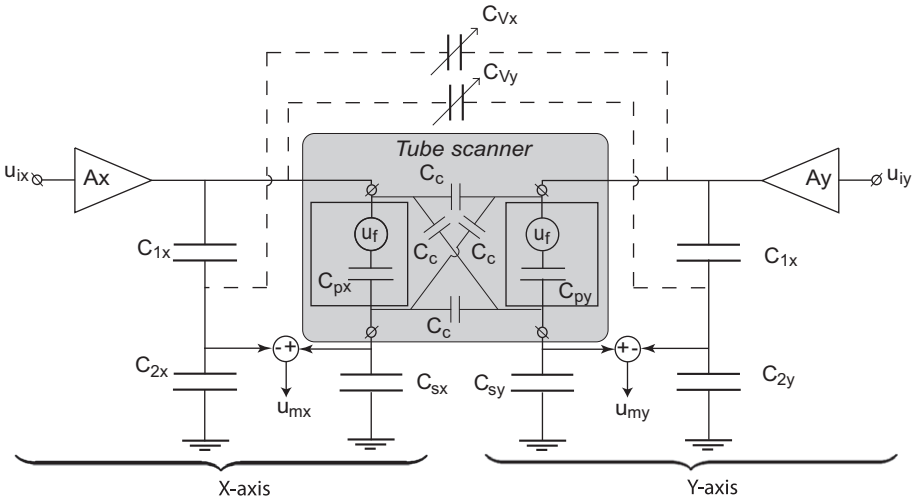

Fig. 3. Scheme of the self-sensing actuation circuit for both scanning axes of a piezoelectric tube scanner.

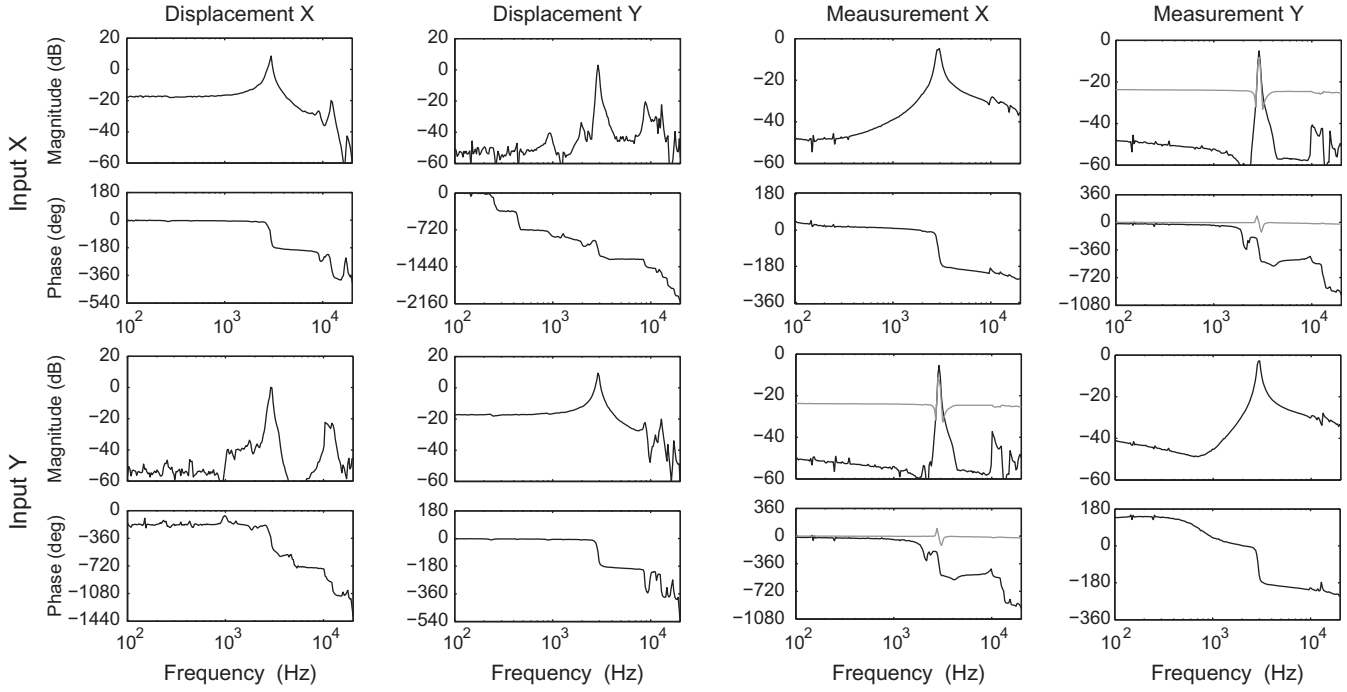

Fig. 4. Frequency response plot of the scanner displacement measured with a vibrometer, and the bridge circuit measurement signals. The grey lines in the off-diagonal responses of the measurement signals show the responses before compensating for the capacitive coupling between both axes and in black, the responses after compensation.

x the actuator displacement, M the total effective mass and β the structural damping within the structure [20]. Accordingly, the voltage measured over the bridge circuit $u_m(t)$ when used on a piezoelectric tube scanner is proportional to a combination of the acceleration and velocity of the actuated mass.

2.2. MIMO implementation of self-sensing tube scanner

The self-sensing capacitive bridge circuitry has been implemented on both scanning axes of a commercially available tube scanner (E-scanner, Veeco, Santa Barbara, USA), according to the scheme in Fig. 3. A more detailed description on the electronic implementation of this circuit is given in Section 5. Measured frequency responses of the tube scanner in both axes are given in Fig. 4 for two sensing methods: using a vibrometer (Polytec, Waldbronn, Germany), and using the self-sensing bridge circuitry. The weakly damped fundamental resonances at 3 kHz can clearly be observed in the frequency responses of the measured scanner displacement, both in the direct responses as well as in the cross-coupling. Fig. 4 shows that these scanner resonances can clearly be resolved in the responses of the measurement signals from the self-sensing bridge circuitry as well. However, as can be seen in Fig. 4 (grey lines), the measurement signals show a strong cross-coupling over all frequencies which is not observed in the responses of the displacement measured with the vibrometer. This cross-talk is caused by the large parasitic coupling capacitances within the piezoelectric tube [21], which are denoted C_c in Fig. 3. This capacitive coupling is stemming from the fact that the electrodes of both individual scanning axes are located closely to each other on the same piezoelectric tube. By measuring the capaci-

tances between the adjacent electrodes on the piezoelectric tube the coupling capacitances are determined to be about 0.4 nF, which amounts to 10% of the capacitances of the active piezo segments, measured to be about 4 nF. This capacitive coupling causes a direct electric feed-through of the driving voltage from one axis towards the measurement signal of the other axis, resulting in a large cross-talk as observed by the grey lines in the off-diagonal response of the measurements signals in Fig. 4.

The capacitive cross-talk in the piezoelectric tube scanner is compensated for by using two additional capacitors, denoted C_{V_y} and C_{V_x} in Fig. 3. These variable capacitors are tuned such that they cancel out the cross-talk of the driving voltage of the *X*- and *Y*-axis towards the measurement signals, reducing the coupling in the measurement signals with up to 30 dB, as clearly can be seen in the frequency responses of the measurement signals in Fig. 4 (black lines). After compensation, a strong coupling in the measurement signals is only observed at the resonance frequencies, which is a true mechanical coupling. As will be discussed in Section 4, the electrical decoupling of the measurements signals allows for decentralized control for active damping of the resonances, which simplifies the controller design and enables a low-cost analog implementation.

3. Bridge circuit imbalance compensation

The frequency responses shown in Fig. 4 are captured with small driving signal amplitudes, in order not to excite the non-linearities of the scanner. For larger signal amplitudes, however, the piezoelectric tube scanner suffers from hysteresis which influences the responses of the scanner displacement and the measurement signals. If not accounted for, the hysteresis within the piezoelectric tube scanner can cause an imbalance in the self-sensing bridge circuit which may effect the integrity of the self-sensing signal. However, this imbalance can be compensated for by an adaptive circuit balancing technique [20].

3.1. Hysteresis induced bridge circuit imbalance

As discussed in [22], the hysteresis within a piezoelectric element occurs as a non-linear relation between the voltage $u_p(t)$ over the piezoelectric element and the resulting charge $q(t)$. The hysteresis can therefore be modeled as a non-linear impedance which is in series with the 'ideal' piezo element as shown in the bridge circuit of Fig. 5. As the hysteresis is not present in the reference capacitors of the bridge circuit, an imbalance in the bridge circuit is introduced, resulting in a differential voltage over the bridge circuit that is depending on the hysteresis induced voltage drop $u_{\mathscr{H}}(t)$ over the piezo element. The measurement signal of Eq. (5) therefore becomes:

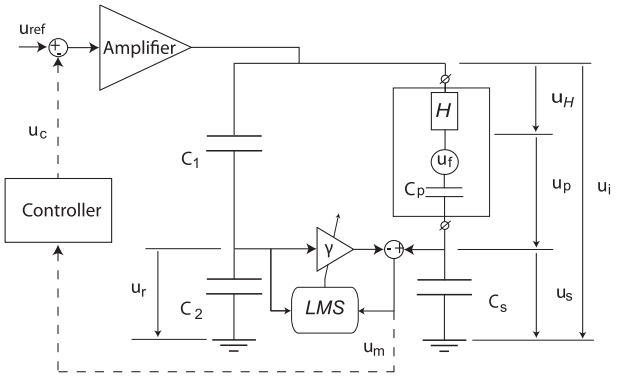

Fig. 5. Scheme of capacitive bridge circuit for self-sensing piezo actuation with adaptive circuit balancing and feedback controller (one axis).

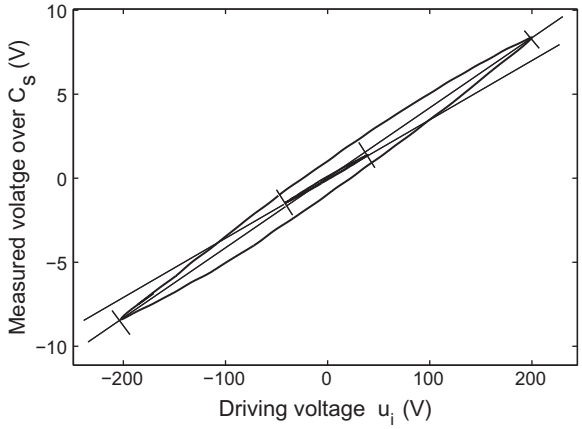

Fig. 6. Measured voltage $u_s(t)$ over capacitor C_s in series with piezo to a 80 V_{pp} and a 400 V_{pp} driving voltage $u_i(t)$. The straight lines illustrate the difference in peak-to-peak gain for the different driving voltage amplitudes.

$$u_m(t) = \frac{C_p}{C_p + C_s} \cdot \left(u_i(t) + \frac{d}{C_p} f_p(t) - u_{\mathscr{H}}(t) \right) - \frac{C_1}{C_1 + C_2} \cdot u_i(t)$$
$$= \frac{C_p}{C_p + C_s} \cdot \left(\frac{d}{C_p} f_p(t) - u_{\mathscr{H}}(t) \right). \quad (6)$$

In most AFM setups the loss in position accuracy due to the hysteresis is compensated in open loop by calibration. When using the measurements signals from the self-sensing bridge circuitry for feedback control in order to dampen the scanner resonances, feedback of the hysteresis induced voltages $u_{\mathscr{H}}(t)$ in the measurement signals must be avoided in order not to interfere with the scanner calibration. Therefore, a circuit balancing technique is used to remove the hysteresis induced voltage $u_{\mathscr{H}}(t)$ in the measurement signal $u_m(t)$. To analyze the hysteresis induced imbalance in the bridge circuit (cf. Fig. 5), the voltage $u_s(t)$ over the capacitor C_s is measured as a function of the amplitude of the scanning signal. Fig. 6 shows the response for two 20 Hz triangular reference signals at an amplitude of 80 V_{pp} and 400 V_{pp}. Hereby it shows that the hysteresis not only causes a curved response, but also a varying peak-to-peak gain for the different driving amplitudes, as is apparent from the different slopes of the hysteresis curves. In the graph of Fig. 7 (solid line) the measured peak-to-peak gain is shown for different driving amplitudes, showing a variation of around 30% from the smallest (30 V_{pp}) to the largest (440 V_{pp}) driving voltage amplitudes. As in

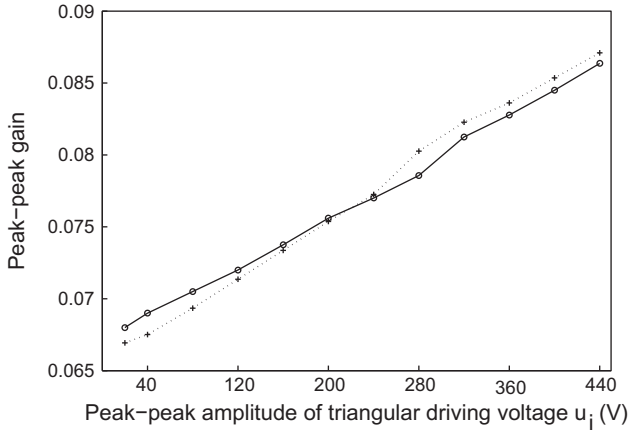

Fig. 7. Peak-to-peak gain u_s/u_i (solid) and $\gamma \cdot u_r/u_i$ (dashed) for different amplitudes of triangular driving voltages (20 Hz), showing that the adaptive gain γ is tracking the gain difference in u_s/u_i.

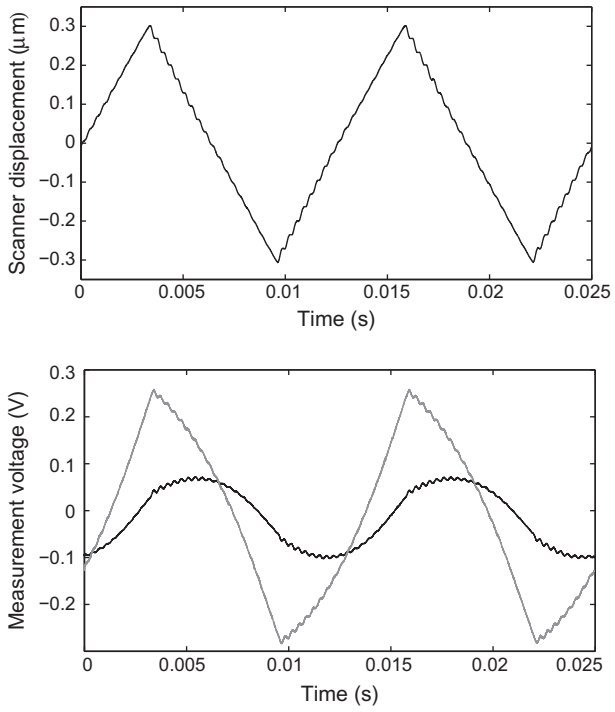

Fig. 8. Response of the system to a 80-Hz triangular reference signal (*X*-axis only). Scanner displacement measured with a vibrometer and measurement signal from the bridge circuit, without (grey) and with (black) adaptive balancing of the bridge circuit. The major part of the hysteresis induced voltage in the self-sensing measurement signal is compensated by the gain adaptation.

AFM-imaging triangular reference signals are used for scanning, the major part of the hysteresis induced voltage $u_{\mathscr{H}}(t)$ in the measurement signal $u_m(t)$ can be canceled by compensating for this variation in the peak-to-peak gain. This compensation is done using an additional gain γ to balance the two branches of the bridge circuit, as depicted in Fig. 5, and adapting its value to optimally balance the bridge circuit for the actual driving voltage.

Fig. 8 shows the vibrometer measurement of scanner displacement in response to a 80 Hz triangular reference signal, and the resulting measurement signal from the self-sensing bridge circuit in the uncompensated case (grey line) and when compensating for the gain variation by balancing the bridge (black line). In the compensated case, the low-frequency components in the measurement signal which are due to the bridge circuit imbalance are significantly reduced. The obtained reduction in bridge circuit imbalance improves the quality of the self-sensing signal and prevents saturation of the sensor signal, which may occur in the operational amplifiers of the sensor electronics due to large hysteresis induced voltage at full scan range. Because adaptation of the gain γ only compensates for the variation of the peak-to-peak gain due to hysteresis, residual components stemming from the curvature of the hysteresis loops (cf. Fig. 6) can still be observed in the measurement signal. However, these components occur at low frequencies in the range of the line scan rate, which is much lower than the resonance frequency. Especially for the larger scan ranges the obtained reduction in circuit imbalance due to the gain adaptation is found to be vital to avoid interference with the scanner calibration when using the measurement signal for feedback control, as is demonstrated experimentally in Section 6. This circuit balancing procedure can be automated by an *LMS*-based adaptive circuit.

3.2. LMS-based gain adaptation

In [23,24] a method is presented to compensate for possible imbalance of the bridge circuit by adaptation of the gain value γ (cf. Fig. 5). The adaptive gain value $\gamma(t)$ is hereby minimizing the Least Mean Square (*LMS*) estimate of the measurement signal $\gamma(t) = \arg\min_\gamma(E[u_m^2(t)])$. The application presented in [23] is to compensate for bridge imbalance due to the change of piezo-capacitance C_p, caused by aging or temperature drift. However, the adaptive bridge circuit balancing can also be used to compensate for the varying peak-to-peak gain caused by the hysteresis of the piezo element [20]. The update law for $\gamma(t)$ is hereby taken as

$$\gamma(t) = \gamma_0 + \gamma_a(t) = \gamma_0 + \frac{\mu}{2}\int \frac{\partial J(t)}{\partial \gamma_a(t)}dt, \tag{7}$$

where γ_0 is the initially set gain value and $\gamma_a(t)$ is the adaptive gain value. The gain value γ_0 is tuned such that it minimizes the feedthough for the linearized system (i.e. for small amplitudes). The factor μ is the learning gain which determines the convergence speed and stability of the adaptation. $J(t)$ is the cost function to be minimized by the adaptation, which is chosen as

$$J(t) = [u_m(t)]^2 - \rho[\gamma_a(t)]^2, \tag{8}$$

where ρ is a leakage gain that is described below. Taking the derivative of $J(t)$ with respect to $\gamma_a(t)$ leads to

$$\frac{\partial J(t)}{\partial \gamma_a(t)} = -(2\cdot u_m(t)\cdot u_r(t) + 2\cdot\rho\cdot\gamma_a(t)), \tag{9}$$

where $u_r(t)$ is the voltage measured over capacitor C_2 (cf. Fig. 5). Substitution in Eq. (7) gives

$$\gamma(t) = \gamma_0 - \mu\int (u_m(t)\cdot u_r(t) + \rho\cdot\gamma_a(t))dt. \tag{10}$$

Eq. (10) shows that at zero input signal ($u_r(t) = 0$), the term $\rho\cdot\gamma_a(t)$ is the only term within the integral. The gain $\gamma_a(t)$ will therefore leak away to zero, hence the term leakage factor for ρ. This addition to the adaptation algorithm described in [23] causes $\gamma(t)$ to converge more rapidly towards γ_0 when changing to a smaller input signal and prevents drifting of $\gamma_a(t)$ when no input signal is applied. The *LMS*-based adaptive circuit balancing is implemented on both scanning axes, as discussed in Section 5. Fig. 7 shows the measured peak-to-peak gain variation in $u_s(t)$ for a low-frequency triangular input signal with varying amplitudes, demonstrating that $u_r(t)\cdot\gamma(t)$ is able to track this gain variation (dashed), to compensate the hysteresis induced imbalance in the bridge circuit. The learning gain μ is set such that when changing the scan range the adaptable gain $\gamma_a(t)$ converges within about 3 s. The learning rate should, however, not be set too high in order to avoid undesirable interference between the *LMS*-based gain adaptation and the actual feedback control for active damping of the resonant modes.

4. Controller design

The objective for the controller is to add damping to the weakly damped resonances of the piezoelectric tube scanner using the measurement signals from the self-sensing bridge circuitry. Fig. 5 (dashed lines) shows the control structure of this control method for one scan axis to feedback the measurement signal of the bridge circuit for active damping. Although the tube scanner is a MIMO system with two inputs (*X* and *Y*) and two self-sensing channels, due to the electrical decoupling of both axes, coupling in the measurement signals is only present at the mechanical resonance frequencies of the tube scanner (cf. Section 2). The decoupling of the sensing circuits allows the use of two decentralized controllers instead of requiring a full MIMO controller, which reduces the complexity of the controller and therefore facilitates a low-cost and low-noise analog implementation of the controller. Due to the symmetry of the tube scanner,

the frequency response of both axes are very similar which allows using the same SISO controller for both scanning axes. As discussed in the previous section, residual low-frequency components of the hysteresis induced voltage drop over the piezo $u_{\mathscr{H}}(t)$ are still present in the measurement signals (cf. Fig. 8). As mentioned also in Section 3, feeding back the components in the measurement signal stemming from the hysteresis should be avoided in order not to interfere with the calibration of the setup where the loss in position accuracy due to the hysteresis is compensated for. Because the residual hysteresis induced components in the measurement signal occur primarily at the frequency of the line scan rate (cf. Fig. 8), which is much lower that the resonance frequency of the tube scanner, the feedback controller should have low gain at these frequencies to attenuate the hysteresis induced components in the measurement signals. Furthermore, the controller should roll-off at higher frequencies to prevent instability due to higher order modes.

For these reasons the controller is chosen as a fourth-order bandpass filter with the following transfer function:

$$C(s) = \alpha \cdot \frac{s^2}{\left(s^2 + 2\zeta \cdot \omega_c + \omega_c^2\right)^2}, \tag{11}$$

where α is a gain factor and ζ and ω_c are the damping and corner frequency of the bandpass filter, respectively. The controller is tuned such that it provides a phase lag of 90° at the resonance frequency of the tube scanner, which resulted in $\omega_c = 7400$ rad/s. The damping of the controller poles is set to $\zeta = 1$ in order to smoothen the phase decay of the controller, adding some robustness to variations in the tube scanner resonance frequencies.

The controllers are implemented as analog circuits, as discussed in Section 5. Fig. 9 shows the measured frequency responses of the loop-gains of both scanning axes. The bandpass behavior of the controllers clearly can be recognized, only applying a high feedback gain at the mechanical resonance frequency of the tube scanner at 3 kHz. As can be seen, the phase of the loop gain is between +90° and −90° at the frequencies where the gain exceeds the 0 dB-line, resulting in a stable closed loop system. The proposed controller may have some similarities with Resonant Controllers [25] when looking at the resulting loop gain, which are typically used for systems where a direct measurement of the actuator displacement is available.

Fig. 10 shows the frequency response of the scanner displacement in the uncontrolled case and with the active damping by the proposed feedback scheme. It clearly shows the significant reduction of the resonance peaks in both scanning axes by 18 dB, and the reduction in cross-coupling at these frequencies of about 30 dB.

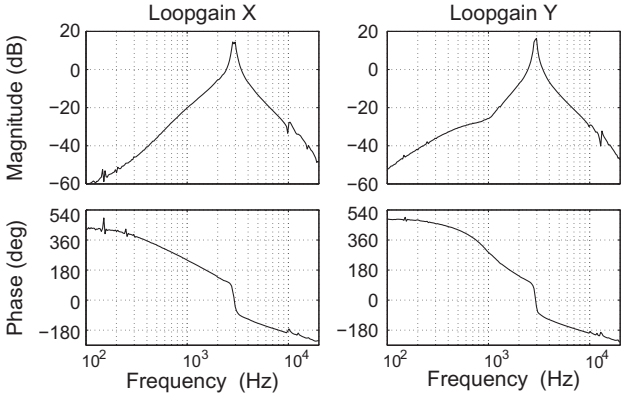

Fig. 9. Frequency responses of the loop-gains of the *X*-axis and the *Y*-axis.

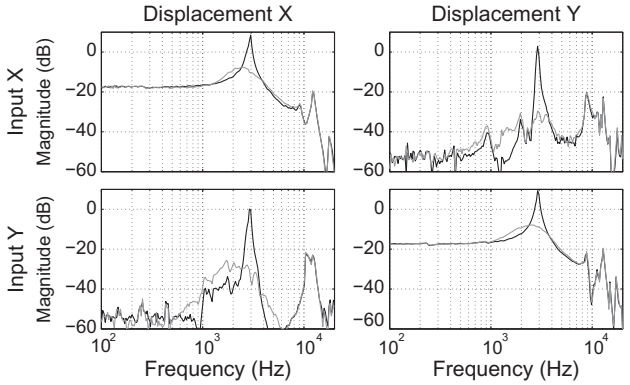

Fig. 10. Frequency response plot of the tube scanner displacement, uncontrolled (black) and controlled (grey).

5. Implementation

The proposed control method is implemented as shown for one axis in Fig. 11. As for the implementation only analog electronics are used, the use of expensive (digital) signal processors is omitted. The implementation of the proposed control method therefore only requires a low-cost modification of the electronics of the conventional AFM system, and leaves all other hardware unchanged.

The bridge circuit, as discussed in Section 2, is implemented using additional resistors in parallel with the capacitors in order to prevent any drift due to the finite input impedance of the buffer amplifier measuring the voltages over capacitors C_s and C_2. The resistor values are chosen such that these do not introduce any additional dynamics to the system by matching the time constants of the resulting low-pass filter. The high voltage amplifier, denoted A_{HV} in Fig. 11, is a dual channel, single ended amplifier (PZD700, Trek, Medina, USA). Variable capacitors C_{V_x} and C_{V_y} are used to compensate for the capacitive coupling between the two scanning axes, as discussed in Section 2.

The *LMS*-based adaptive circuit balancing, described in Section 3, is implemented using two multipliers (AD663) and one operational amplifier. The nominal gain value γ_0 of the adaptation (cf. Section 3) is set using variable resistor R_{V_1}, the leakage gain ρ using variable resistor R_{V_2}, and the learning gain μ using variable resistor R_{V_3}.

The bandpass filter for the feedback controller is implemented using two operational amplifiers, where the feedback gain is set using variable resistor R_{V_5}. A switch S_1 is used to enable and disable the feedback control action. A summing stage, made using one operational amplifier, adds the reference signal $u_{ref}(t)$ and control signal $u_c(t)$ forming the input signal for the high voltage amplifier.

6. Experiments

In order to demonstrate the improved system performance by the proposed control method, the system responses to triangular reference signals of different amplitudes and frequencies are measured, and AFM images are recorded to show the reduction in image distortion.

6.1. Line scan experiments

To examen the reduction in scanner oscillations due to the proposed control method, the systems response is measured when scanning with a triangular reference signal at varying scan-frequencies and amplitudes. The results are shown in Fig. 12 for scanning in the *X*-axis at a line scan frequency of 60 Hz (a, c, e, and g)

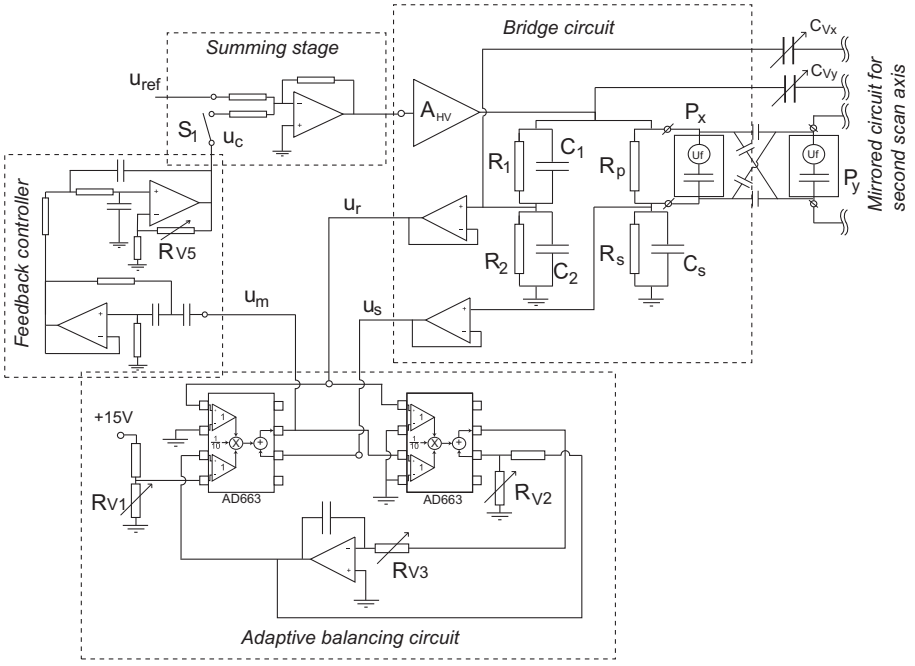

Fig. 11. Analog implementation of self-sensing actuation and control of a piezoelectric tube scanner of one scanning axis. Switch S_1 open corresponds to the uncontrolled case and S_1 closed corresponds to the actively damped case.

and 120 Hz (b, d, f, and h), and a driving voltage amplitudes of 50 V_{pp} (a and b), 200 V_{pp} (c and d) and 500 V_{pp} (e and f), respectively. Also the response of the un-actuated *Y*-axis is shown while scanning the *X*-axis with a 200 V_{pp} driving voltage (g and h).

Each set of graphs shows the scanner displacement (index 1) and velocity (index 2) measured with a vibrometer, the measurement signal from the bridge circuit (index 3) and the feedback signal, i.e. the output signal of the controller (index 4). In each set of graphs the response of the system is shown for the uncontrolled case (red), where the feedback loop is disconnected via switch S_1 (cf. Fig. 11), and for the controlled case (blue), i.e. with active damping.

In the uncontrolled cases (red), the oscillations of the scanner are visible in the displacement and velocity signals, as well as in the measurement- and controller signals. These oscillations last over the entire scan line for both scanning speeds. In the actively damped cases, the oscillations are clearly damped stronger, and occur only at the begin of the scan line where the scanning motion is reversed.

In Fig. 12g and h the responses of the system is shown in the un-actuated *Y*-axis, while the *X*-axis is driven by a 200 V_{pp} triangular reference signal of 60 Hz (g) and 120 Hz (h). In the uncontrolled case the coupling induced oscillations are clearly visible, while in the controlled case these oscillations are significantly reduced.

Although an adaptive circuit balancing techniques is used to compensate for most of the bridge circuit imbalance caused by the hysteresis (cf. Section 3), the measurement signals still show a residual low-frequency component as is visible in Fig. 12c3–f3. As discussed in Section 3, feeding back these low-frequency components in the measurement signals should be avoided in order not to interfere with the scanner calibration. Although the controllers have strong high-pass characteristics, a small part of the low-frequency components in the measurements signals still enter the control signals as can be seen in Fig. 12c4–f4. This effect becomes more prominent for the larger scan ranges and at higher scan frequency. For the smaller scan ranges a small jump can be observed in the control signal only at the beginning of each line scan (a4, b4), whereas for the larger scan range (e4, f4) the low-frequency components in the control signal last over the whole line scan. Fig. 12 also reveals that the scanner oscillations are damped out slightly faster for smaller scan ranges as compared to the larger scan ranges, which maybe caused by variations in the loop gain due to the hysteresis in the piezo elements and due to the adaptive bridge circuit balancing [20]. Nevertheless, in all cases the scanner oscillations are significantly reduced by the proposed control method as compared to the uncontrolled tube scanner, enabling AFM-imaging at high speeds.

6.2. AFM-imaging

To demonstrate the improvement in image quality, AFM images of a 476 nm line pitch calibration grating are obtained with the uncontrolled and the controlled tube scanner. In order to show the true benefit of controlling both axis of the tube scanner, the images shown in Fig. 13 are obtained while scanning at an image rotation of 45°. Therefore, the reference signals $r_x(t)$ for the *X*-axis and $r_y(t)$ *Y*-axis are given as:

$$r_x(t) = \cos\left(\frac{\pi}{4}\right) \cdot r_f(t) - \sin\left(\frac{\pi}{4}\right) \cdot r_s(t),$$
$$r_y(t) = \cos\left(\frac{\pi}{4}\right) \cdot r_f(t) + \sin\left(\frac{\pi}{4}\right) \cdot r_s(t),$$

where $r_f(t)$ and $r_s(t)$ are the triangular signals for the fast and slow scanning axis, respectively. Note that due to the image rotation the reference signals of both axis are a summation of two triangular signals of different frequency, corresponding to the line scan rate ($r_f(t)$) and the frame rate ($r_s(t)$). As discussed in Section 3, the compensation for the peak-to-peak gain variation due to the hysteresis only works for pure triangular reference signals. Note, however, that the triangular reference signal for the slow scanning axis is at such low frequency that any hysteresis induced imbalance in the bridge circuit due to this low-frequency reference signal will be effectively attenuated by the high-pass characteristic of the controller. Therefore, it is sufficient to let the adaptive circuit balancing only learn the peak-to-peak gain variation due to the fast triangular reference signal $r_f(t)$. This peak-to-peak gain variation appears to be

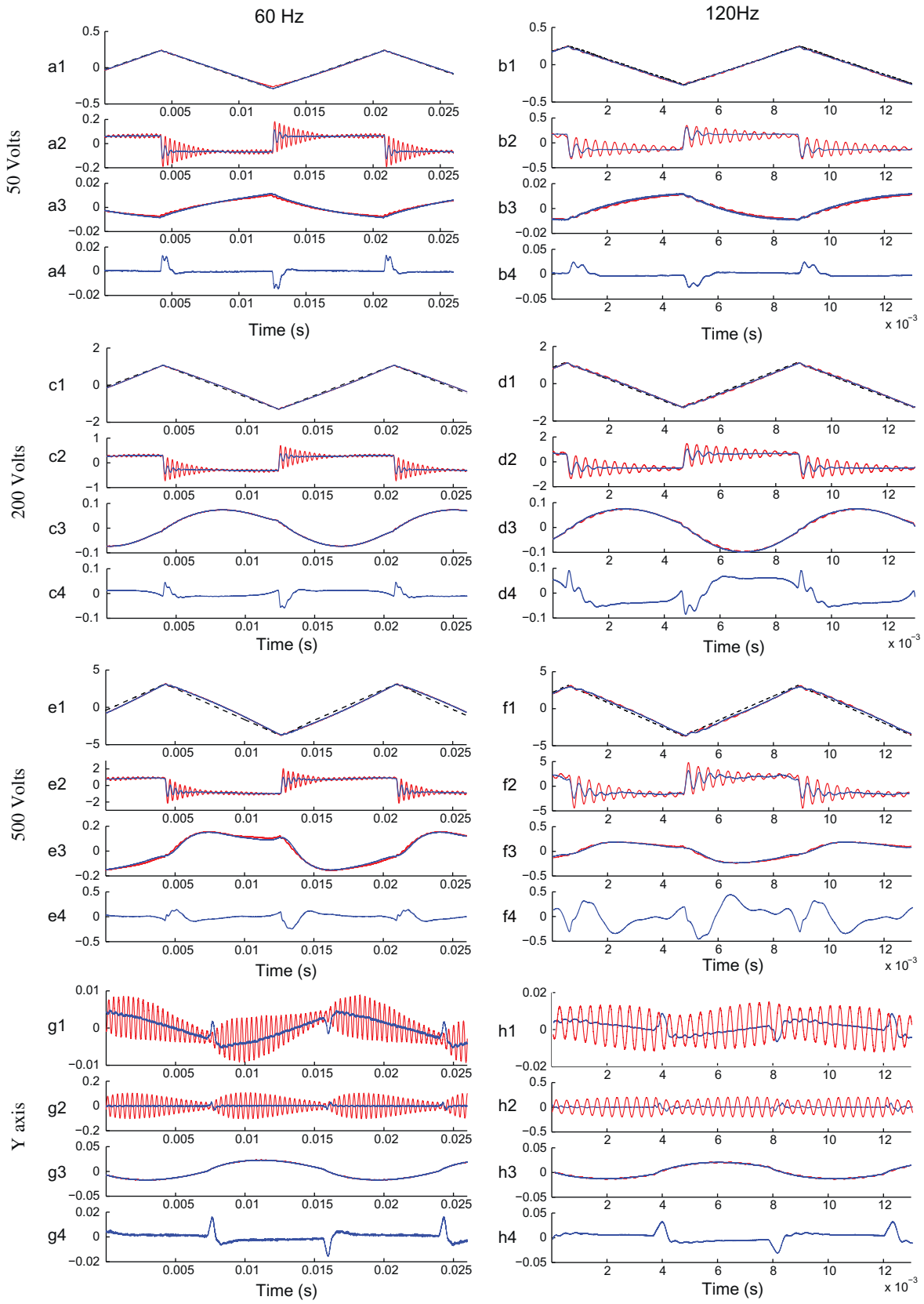

Fig. 12. Response of the system while driving the system with a triangular driving signal of 60 Hz (left) and 120 Hz (right) of varying amplitudes. Each set of graphs shows the scanner displacement [μm] (1), scanner velocity [mm/s] (2), measurement signal from bridge circuit [V] (3) and control signal from the controller [V] (4) in the uncontrolled (blue) and controlled case (red). The lower sets of graphs shows the uncontrolled and controlled response in the un-actuated *Y*-axis, while driving the *X*-axis with a 200 V triangular driving signal of 60 Hz and 120 Hz.

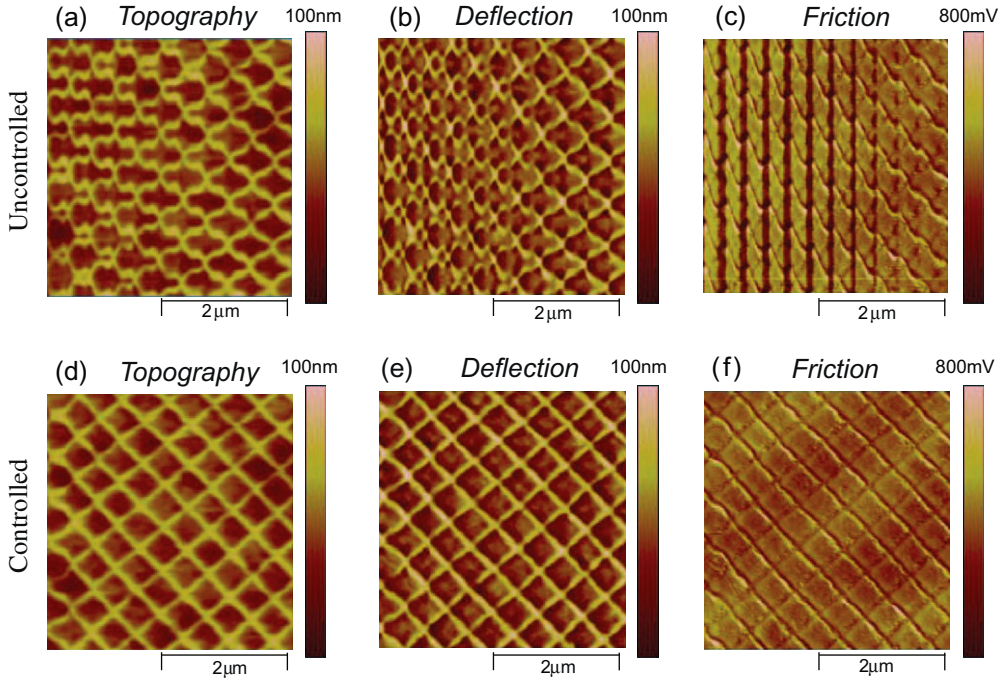

Fig. 13. AFM images of a calibration grid with line pitch of 0.476 μm, scanned with at an image rotation 45° and at a line scan speed of 122 Hz. The resolution of the images is 256 × 256 pixels. The upper images are captured with the uncontrolled system and the bottom images are captured using the proposed control method for active damping of the tube scanner.

largely independent to any offsets. Therefore, when scanning at an image rotation first the optimal adaptive gain γ_a has to be learned for the fast triangular reference signal by the *LMS*-adaptation and then fixed, before applying the slow triangular reference signal $r_s(t)$ to the system.

The resulting images are shown in Fig. 13 for the uncontrolled and controlled case. The fast scanning direction corresponds to the horizontal lines in the images, where the left side is the beginning of each scan line. In the uncontrolled case (a–c), the image distortion caused by the scanner oscillations can clearly be recognized by the non-straightness of the grid-lines (a and b) which stretches throughout the whole images. Also in the friction image (c) vertical lines can be observed which are a result of the non-constant tip-velocity over the sample caused by the scanner oscillations [4].

In the controlled case (d–f), the slight image distortion is only visible at the beginning of each scan line (left part of the images), and the vertical lines in the friction image due to variations in the scanning speed are disappeared. This demonstrates that the image quality is significantly improved by the proposed control method for AFM-imaging at high speeds.

7. Conclusions

This contribution demonstrates active damping of the mechanical resonances of a piezoelectric tube scanner in both scanning axis by self-sensing actuation. The scan-electrodes for both scanning axes of the tube scanner are therefore connected in capacitive bridge circuits, which allows to use the same piezo material for actuation and sensing simultaneously. Compensation of hysteresis induced imbalance in the bridge circuit is demonstrated by adapting a variable balancing gain for each line scan amplitude, which is automated by a *LMS*-based adaptation circuit. Using the obtained measurement signals for feedback control enables active damping of the mechanical resonances of the tube scanner with up to 18 dB, and a damping of the mechanical coupling at these frequencies by 30 dB. Experimental results verify a significant reduction of scanner oscillations when applying triangular reference signals to the scanner, and a significant reduction in image distortion when using the controlled tube scanner for AFM-imaging. Implementation of the proposed control method only requires a small modification of the AFM electronics and leaves all other AFM hardware unchanged. Therefore the proposed control method is a very cost efficient way of adding damping to the mechanical resonances of the tube scanner for AFM-imaging and other scanning probe systems.

Acknowledgments

This work is supported by TU Delft faculty Grant PAL-614, by the Netherlands Organization for Scientific Research (NWO) under Innovational Research Incentives Scheme (VENI DOV.7835), and by the National Institutes of Health under Award R01 GM 065354.

References

[1] Binnig G, Quate C, Gerber C. Atomic force microscope. Phys Rev Lett 1986;56(9):930–3.
[2] Binnig G, Smith D. Single-tube three-dimensional scanner for scanning tunneling microscopy. Rev Sci Instrum 1986;57:1688–98.
[3] Croft D, Shed G, Devasia S. Creep, hysteresis, and vibration compensation for piezoactuators: atomic force microscopy applications. AMSE J Dyn Syst, Meas, Control 2001;123:35–43.
[4] Schitter G, Stemmer A. Identification and open-loop tracking control of a piezoelectric tube scanner for high-speed scanning-probe microscopy. IEEE Trans Control Syst Technol 2004;12:449–54.
[5] Ando T, Kodera N, Takai E, Maruyama D, Saito K, Toda A. A high-speed atomic force microscope for studying biological macromolecules. Proc Natl Acad Sci 2001;98(22):12468–72.
[6] Hansma P, Schitter G, Fantner G, Prater C. High speed atomic force microscopy. Science 2006;314:601–2.
[7] Devasia S, Eleftheriou E, Moheimani S. A survey of control issues in nanopositioning. IEEE Trans Control Syst Technol 2007;15:802–23.
[8] Butterworth J, Pao L, Abramovitch D. A comparison of control architectures for atomic force microscopes. Asian J Control 2009;11(2):175–81.
[9] Leang K, Devasia S. Design of hysteresis-compensating iterative learning control for piezo-positioners: applications to atomic force microscope. Mechantronics 2006;16:141–58.

[10] Schitter G, Thurner P, Hansma P. Design and input-shaping control of a novel scanner for high-speed atomic force microscopy. Mechatronics 2008; 18(5–6):282–8.
[11] Tamer N, Dahleh M. Feedback control of piezoelectric tube scanners. In: Proceedings of the 33rd IEEE conference on decision and control, vol. 2; 1994.
[12] Salapaka S, Sebastian A, Cleveland J, Salapaka M. High bandwidth nano-positioner: a robust control approach. Rev Sci Instrum 2002;73:3232.
[13] Sebastian A, Salapaka S. Design methodologies for robust nano-positioning. IEEE Trans Control Syst Technol 2005;13(6):868–76.
[14] Bhikkaji B, Ratnam M, Fleming A, Moheimani S. High performance control of piezoelectric tube scanners. IEEE Trans Control Syst Technol 2007;15:853–66.
[15] Moheimani S, Yong Y. Simultaneous sensing and actuation with a piezoelectric tube scanner. Rev Sci Instrum 2008;79:073702.
[16] Fleming A, Moheimani S. Sensorless vibration suppression and scan compensation for piezoelectric tube nanopositioners. IEEE Trans Control Syst Technol 2006;14:33–44.
[17] Aphale S, Fleming A, Moheimani S. High speed nano-scale positioning using a piezoelectric tube actuator with active shunt control. Micro Nano Lett 2007;2(1):9–12.
[18] Dosch J, Inman D, Garcia E. A self-sensing piezoelectric actuator for collocated control. J Intell Mater Syst Struct 1992;3:166–85.
[19] IEEE standard on piezoelectricity, ANSI/IEEE Standard 176; 1987.
[20] Kuiper S, Schitter G. Self-sensing actuation and damping of a piezoelectric tube scanner for atomic force microscopy. In: Proceedings of the European control conference 2009; 2009.
[21] Kuiper S, Schitter G. Mimo self-sensing actuation of a piezoelectric tube scanner. In: Proceedings of the ASME dynamic system control conference 2009; 2009.
[22] Goldfarb M, Celanovic N. Modeling piezoelectric stack actuators for control of micromanipulation. IEEE Control Syst Mag 1997;17(3):69–79.
[23] Cole D, Clark R. Adaptive compensation of piezoelectric sensoriactuators. J Intell Mater Syst Struct 1994;5:665–72.
[24] Vipperman J, Clark R. Implementation of an adaptive piezoelectric sensoriactuator. Asian J Control 1996;34:2102–9.
[25] Moheimani S, Vautier B. Resonant control of structural vibration using charge-driven piezoelectric actuators. IEEE Trans Control Syst Technol 2005;13(6): 1021–35.